Received: 17 January 2023 | Accepted: 22 May 2023

DOI: 10.1111/1462-2920.16434

RESEARCH ARTICLE

ENVIRONMENTAL MICROBIOLOGY Applied Microbiology International

Unbalancing Zur (FurB)-mediated homeostasis in *Anabaena* sp. PCC7120: Consequences on metal trafficking, heterocyst development and biofilm formation

Irene Olivan-Muro[1] | **Cristina Sarasa-Buisan**[1] | **Jorge Guio**[1] | **Jesús Arenas**[2] | **Emma Sevilla**[1] | **Maria F. Fillat**[1]

[1]Department of Biochemistry and Molecular and Cellular Biology, Faculty of Sciences and Institute of Bioinformatics and Physical of Complex Systems, University of Zaragoza, Zaragoza, Spain

[2]Department of Animal Pathology, Unit of Microbiology and Immunology, Faculty of Veterinary, University of Zaragoza, Zaragoza, Spain

Correspondence
Maria F. Fillat, Department of Biochemistry and Molecular and Cellular Biology, Faculty of Sciences and Institute of Bioinformatics and Physical of Complex Systems, University of Zaragoza, Zaragoza, Spain.
Email: fillat@unizar.es

Funding information
Gobierno de Aragón, Grant/Award Number: E35_20R; Ministerio de Ciencia, Innovación y Universidades, Grant/Award Number: 438 PID2019-104889GB-I00

Abstract

Zinc is required for the activity of many enzymes and plays an essential role in gene regulation and redox homeostasis. In *Anabaena* (*Nostoc*) sp. PCC7120, the genes involved in zinc uptake and transport are controlled by the metalloregulator Zur (FurB). Comparative transcriptomics of a *zur* mutant (Δ*zur*) with the parent strain unveiled unexpected links between zinc homeostasis and other metabolic pathways. A notable increase in the transcription of numerous desiccation tolerance-related genes, including genes involved in the synthesis of trehalose and the transference of saccharide moieties, among many others, was detected. Biofilm formation analysis under static conditions revealed a reduced capacity of Δ*zur* filaments to form biofilms compared to the parent strain, and such capacity was enhanced when Zur was overexpressed. Furthermore, microscopy analysis revealed that *zur* expression is required for the correct formation of the envelope polysaccharide layer in the heterocyst, as Δ*zur* cells showed reduced staining with alcian blue compared to *Anabaena* sp. PCC7120. We suggest that Zur is an important regulator of the enzymes involved in the synthesis and transport of the envelope polysaccharide layer, influencing heterocyst development and biofilm formation, both relevant processes for cell division and interaction with substrates in its ecological niche.

INTRODUCTION

Zinc is an essential nutrient for proper growth, development and cell communication in all forms of life. It is present as a cofactor in all six classes of enzymes, as well as in many proteins and transcription factors (Decaria et al., 2010). Although zinc is considered a redox-inert cofactor, it regulates many aspects of redox biology in the cell (Maret, 2019). Zinc is often involved in the protection of cysteines preventing their oxidation and, in turn, protein inactivation (Cremers & Jakob, 2013). Therefore, any redox change affecting zinc-coordinated thiols will modify the concentration of free zinc in the cell, enabling it to transduce the redox signal. The ability of zinc to work as a signalling molecule is likely due to the specificity and high affinity of protein binding sites for this cofactor, whose concentration as a free ion in the cytosol is extremely low, ranging between nanomolar and femtomolar (Maret, 2006; Outten & O'Halloran, 2001).

Cyanobacteria are photosynthetic prokaryotes broadly distributed in marine, freshwater and terrestrial environments. Their ability to carry out oxygenic

Irene Olivan-Muro and Cristina Sarasa-Buisan have contributed equally to this study.

photosynthesis transformed the biology and chemistry of our planet. Nowadays, cyanobacteria largely contribute to the global carbon and nitrogen cycles and determine the primary productivity of the oceans (Sánchez-Baracaldo et al., 2022). As most bacteria, cyanobacteria rely on zinc for the synthesis and activity of hundreds of proteins, including carboxysomal carbonic anhydrases, ABC-type zinc uptake systems, proteins involved in the intracellular handling of zinc, cyanobacterial DNA ligase, and a large number of hydrolytic enzymes necessary in all catabolic pathways, such as alkaline phosphatase, among others. Furthermore, zinc is also associated in the earliest forms of life with the activities of RNA enzymes, being present in modern t-RNA synthetases (Blindauer, 2008; Decaria et al., 2010; Palenik et al., 2003).

Since cyanobacteria colonize an ample range of environments, they have to deal with nutrient limitations, including zinc, in open ocean oligotrophic environments. Different studies evidenced the involvement of iron and zinc in carbon cycling, since co-limitation of both nutrients in phytoplankton, where cyanobacteria play a dominant role, has been demonstrated (Barnett et al., 2014; Morel et al., 1994). Conversely to what happens in ocean waters, soil and fresh-water cyanobacteria often have to adapt to polluted environments as a result of the increasing anthropogenic activity, where zinc levels can be toxic. Indeed, high zinc concentrations cause a decline in the photosynthetic performance, as well as morphological and ultrastructural modifications in unicellular cyanobacteria, and it has been related to the increase of cyanotoxin production in cyanobacterial blooms (De Magalhães et al., 2004; Perez & Chu, 2020). To cope with the excess of zinc, tolerance mechanisms include reduced nitrogen fixation and alterations in energy metabolism and transcriptional/translational proteins, as well as upregulation of antioxidative proteins for detoxifying reactive oxygen species and the enhanced expression of the systems to chelate free zinc ions (Chakraborty et al., 2022). Thus, considering these results and the occurrence of zinc in a wide variety of enzymes and proteins, it is not surprising that the misregulation of zinc homeostasis can alter diverse metabolic pathways in the cell.

In the nitrogen-fixing cyanobacterium *Anabaena* sp. PCC7120 (also known as *Nostoc* sp. PCC7120), the acclimation to zinc deficiency is controlled by the Zur (FurB) protein encoded by *all2437* (Napolitano et al., 2012). Zur has been found to sense both zinc and redox conditions, playing a remarkable role in the oxidative stress defence in *Anabaena* (Sein-Echaluce et al., 2014; Sein-Echaluce et al., 2018). Previous analysis revealed that Zur controls a large variety of genes (Napolitano et al., 2012; Sein-Echaluce et al., 2014). Consequently, we speculated that disruption of Zur-controlled homeostasis would produce alterations in numerous metabolic pathways that may have relevant consequences for the biology of the cyanobacteria. Therefore, in this work, we have analysed the transcriptome of a *zur* deletion mutant to unveil novel metabolic networks affected by zinc deregulation. Indeed, our results showed that the lack of Zur not only affects the expression of genes involved in metal homeostasis but also the transcription of a large number of genes involved in desiccation tolerance and exopolysaccharide synthesis and transport. Furthermore, a Zur indirect effect on the frequency and the proper development of heterocysts is reported.

MATERIALS AND METHODS

Bacterial strains and culture conditions

Strains used in this work were the wild-type *Anabaena* sp. PCC7120, as well as the genetically modified strains VCS2770 and Δ*zur*. The Δ*zur* strain is a deletion–insertion mutant with a C.S3 cassette interrupting the *zur* gene (Napolitano et al., 2012). The VCS2770 strain is a *zur*-overexpressing strain containing the pAM2770*zur* plasmid, which harbours a *zur* gene behind a copper-inducible *petE* (plastocyanin) promoter (Sein-Echaluce et al., 2014). All cyanobacterial cultures were grown photoautotrophically in BG11 or $BG11_0$ (BG11 lacking a source of combined nitrogen) at 28°C under constant illumination of 30 μE m^{-2} s^{-1} in an orbital shaker at 130 rpm unless otherwise stated. Cultures of strains VCS2770 and Δ*zur* contained 50 μg·mL^{-1} of neomycin (Sigma-Aldrich) and 2 μg mL^{-1} of streptomycin and spectinomycin (Sigma-Aldrich), respectively. As the copper concentration present in BG11 has been described to be sufficient to drive Zur overexpression from the *petE* promoter, no exogenous copper was added to the VCS2770 cultures (Gonzalez et al., 2010).

RNA extraction and sequencing

Total RNA was prepared from three independent cultures of *Anabaena* sp. PCC7120 and the Δ*zur* mutant. Cells from late-log cultures were diluted to an OD_{750nm} of 0.18 in 80 mL of fresh BG11 medium in 250 mL Erlenmeyer flasks and were grown for 6 days to an OD_{750nm} of 0.7 as described above. Then, cells were harvested by centrifugation, and RNA was extracted following a method previously described (Sarasa-Buisan et al., 2022). RNA seq was performed by STAB VIDA Lda (Lisbon, Portugal) from total RNAs extracted and processed from two RNA biological replicates of *Anabaena* sp. PCC7120 and Δ*zur* cultures. The library construction of cDNA molecules was carried out using a Ribosomal Depletion Library Preparation Kit 'NEBNext rRNA Depletion Kit followed by Roche KAPA

Hyperprep' following the manufacturer's instructions. The pool of libraries was sequenced in the Illumina Novaseq platform, using 150 bp paired-end sequencing reads. The samples generated contained 28,578,796–42,133,876 sequence reads. The RNA sequencing data are available in ArrayExpress with the accession number E-MTAB-12347.

Bioinformatic analyses

The analysis of the generated raw sequence data was carried out by STAB VIDA Lda (Portugal) including the following pipeline: Quality control of raw readings was performed with the FastQC tool (http://www.bioinformatics.babraham.ac.uk/projects/fastqc/), trimming, mapping and expression analysis performed using CLC Genomics Workbench 12.0.3, (n.d.). The trimming can be divided into quality trimming based on quality scores (0.01), ambiguity trimming (two nucleotides), and length trimming (minimum of 15 bp). The expression levels for all samples were accessed through the mapping of the high-quality reads of each sample against the *Nostoc* sp. PCC 7120 = FACHB-418 (GCA_000009705.1) reference genome. Statistical significance was considered for false discovery rate (FDR) corrected *p*-value ≤0.05 and a fold change (≥2 or ≤−2). Differentially expressed genes (DEGs) were subjected to a search in literature and the databases Cyanobase (Fujisawa et al., 2017) and KEGG (Kanehisa et al., 2022) to annotate gene symbols and protein function.

To facilitate the search for Zur direct target candidates among the total DEGs, we analysed the presence of putative Zur-DNA binding motifs in the promoter regions of DEGs identified by RNA-seq. In cases where the DEGs were included in operons, either described in the literature or predicted according to the MicrobesOnline operon information tool (Alm et al., 2005), the promoter region of the first gene of the operon was also investigated. While the presence of a predicted binding box does not guarantee direct Zur regulation, this was used as a selection criterion to narrow down the list of candidate genes for which to carry out binding assays. For this purpose, a Zur-binding position-weight-matrix was generated by MEME (http://meme-suite.org/tools/meme) (Bailey et al., 2006) using the FASTA sequences of the 15-bp FurB-DNA binding sites described previously (Napolitano et al., 2012) with the default parameters (Figure S1). The obtained Zur-matrix was used as the input for FIMO analyses (http://meme-suite.org/tools/fimo) (Grant et al., 2011) to identify best matches within the selected promoter sequences with a cut-off of a *p*-value $<1 \times 10^{-4}$. The promoter sequences were retrieved manually from the KEGG database (Kanehisa et al., 2022), selecting sequences from −500 to +50 bp with respect to the start codon.

Real-time RT-PCR

A 2 μg of total RNA was reverse-transcribed using SuperScript retrotranscriptase (Invitrogen) following the manufacturer's conditions. Real-time PCR was performed using the QuantStudio 5 system (Applied Biosystems). Each reaction was set up by mixing 12.5 μL of SYBR Green PCR Master Mix with 0.4 μL of 25 μM primer mixture and 10 ng of cDNA template in a final volume of 30 μL in nuclease-free water (Ambion), with additional water added instead of cDNA for negative controls. Amplification was performed at 60°C for 40 cycles. The sequences of specific primers of selected genes were designed with Primer Express 3 (Thermofisher) and are given in Table S1. For the normalization of transcripts levels, the housekeeping gene *rnpB* was used (Vioque, 1992). Relative quantification and expression fold changes were calculated according to the comparative Ct method (ΔΔCt method) (Livak & Schmittgen, 2001), where the fold change threshold was set up to ≥1.5 or ≤−1.5.

Electrophoretic mobility shift assay

DNA fragments for electrophoretic mobility shift assay (EMSA) were obtained by PCR, using the *Anabaena* sp. PCC7120 genome as template and primer pairs given in Table S1 to amplify the 250–350 bp promoter regions of selected genes. EMSA was performed using a recombinant Zur (FurB) purified as previously described (Sein-Echaluce et al., 2018). Briefly, recombinant Zur was produced in *Escherichia coli* BL21 cells transformed with a pET-28a(+) plasmid (Novagen) containing the *zur* gene sequence followed by a His-tag. Protein production was induced with 1 mM IPTG, and then cells were harvested by centrifugation, resuspended in the appropriate buffer and sonicated, and the cell debris was removed by an additional centrifugation step. The resulting supernatant was loaded into a Chelating Sepharose Fast Flow column previously loaded with zinc. After a 0–1 M imidazole gradient elution step, the purest fractions were dialyzed against 10 mM acetic acid/acetate buffer pH 5.5 and then stored at −20°C.

Samples containing 50 ng of promoter DNA were incubated at room temperature for 30 min with different concentrations of Zur in a binding buffer containing 10 mM Bis Tris-HCl, pH 7.5, 40 mM KCl, 0.1 mg ml^{-1}, BSA, 1 mM of 1,4-dithiothreitol (DTT), 5 μM $ZnSO_4$ and 5% (vol/vol) of glycerol, in a final volume of 20 μL per sample. To probe non-specific binding a competitor DNA was used, which consisted of 50 ng of the internal fragment of gene *pkn22* (if*pkn22*). Then, samples were mixed with a 6× loading buffer (containing 30 mM Bis-Tris pH 8, 30% glycerol, and 0.05% bromophenol blue), loaded into a non-denaturing 6% polyacrylamide gel, and ran at 4°C under a voltage of 90 V for

approximately 110 min. Gels were stained with SYBR® Safe (Invitrogen) and visualized in a GelDoc 2000 device (Bio-Rad).

Inductively coupled plasma-mass spectrometry

Cyanobacterial samples for intracellular metal concentration analysis were obtained from cultures grown under standard culture conditions in Roux bottles. Approximately 900 mL of late-log cultures of each strain were centrifuged and the resulting pellets were washed three times with Sörensen buffer (66 mM KH_2PO_4, 66 mM Na_2HPO_4, pH 7.1) to eliminate medium culture traces. Cell pellets were freeze-dried in a Christ Alpha 1–4 LSC lyophilizer for a final yield of approximately 250 mg per culture, with three independent cultures per strain. Metal quantification was carried out by the Servicio de Ionómica from CEBAS-CSIC (Murcia, Spain).

Microscopy assays

Microscopy observations were carried out through both bright field and fluorescence microscopy using a Nikon Eclipse 50i Epi-fluorescence microscope coupled to a Nikon DXM 1200F camera. Fluorescence microscopy was observed for intrinsic phycobiliprotein fluorescence.

Heterocyst development and counting

For heterocyst development analysis, log phase cultures (OD_{750nm} ranging from 0.7 to 1.0) of *Anabaena* strains PCC7120, VCS2770 and Δ*zur* were used. To reduce traces of combined nitrogen to a minimum, cells were washed three times with $BG11_0$ by centrifugation and then cultures were adjusted to an OD_{750nm} of 0.5 in 100 mL of culture medium in 250 mL Erlenmeyer flasks. Then, cells were cultivated for 72 h in otherwise standard culture conditions. Heterocyst percentage values were obtained through a combination of manual and automated counting using image processing software ImageJ 1.53e (Schneider et al., 2012). Vegetative cell counts were estimated via cell surface measurements to avoid false lower counts derived from the image processing of filaments that are in contact with each other. Intrinsic fluorescence microscopy images were used due to their higher contrast and ability to exclude heterocysts, which lack fluorescent photosynthetic pigments, under the appropriate threshold. Micrographs were processed as follows: first, the image type was adjusted to 8-bit, a threshold was applied to select only the filaments and the resulting images were processed into binary. Then, the measurement tool was used to obtain a value of the total cellular surface in pixels per field. In parallel, average single-cell surface values were determined based on isolated filaments for a minimum of 2000 cells per strain and experiment. For this purpose, individual cells were marked in each micrograph using the watershed tool. Next, the analyse particles tool was applied with a 1500–6000 pixel size limit and 0.2–1 circularity, to discard non-representative aggregates and cell fragments. This tool returns the surface value in pixels of all isolated cells, which was used to obtain the average values for each nitrogen-deprived strain. The number obtained after dividing each field's total surface value by their corresponding average cellular surface represents the estimated vegetative cells contained in the field. On the other hand, the number of heterocysts was determined by manual counting based on cell morphology and lack of intrinsic fluorescence. The heterocyst percentage indicates which fraction these cells represent over the sum of vegetative and heterocyst cells present in all fields considered. The resulting heterocyst percentages from three independent assays were used to obtain a mean value for each strain, with a minimum of 10000 estimated cells counted in total per strain.

Heterocyst and proheterocyst staining

Alcian blue was used to visualize the heterocyst (and proheterocyst) polysaccharide layers (McKinney, 1953). For each strain, a volume of 500 μL of nitrogen-deprived cultures, grown under the same conditions used for heterocyst counting, was used. Cells were concentrated by centrifugation at 3000 rpm for 5 min at room temperature, resuspended in 20 μL $BG11_0$, and mixed at a 5:1 ratio with alcian blue 1% (Alcian Blue 8GX, Panreac), previously filtered through a 0.45 μm cellulose acetate syringe filter (Branchia). After 5 min, samples were diluted by the addition of 200 μL of $BG11_0$ and mounted for microscopy visualization.

Biofilm formation assays

For biofilm formation experiments, cyanobacteria from log phase BG11 cultures were adjusted to an OD_{750nm} of 0.3. Samples of 300 μL per well were seeded into uncoated Ibidi μ-Slide 8-well high-chambered coverslips, and incubated under static conditions, 10 μE of light, and 28°C for 10 days. Plate lids were secured with parafilm to reduce evaporation. To assess biofilm formation by the different cultures, the planktonic fraction was removed along with cells not tightly adhered to the substrate, each well was stained for 2 min with 0.25% (wt/vol) crystal violet (Merck) and washed three

times to remove excess dye and visualize cells most tightly adhered to the substrate and their biofilm matrix. The amount of biofilm was evaluated by image quantification of the intensity of crystal violet-stained biofilms using image processing software ImageJ 1.53e (Schneider et al., 2012). Biofilm biomass was expressed as the obtained raw integrated density values measured in each individual well after background subtraction. For each mutant, this value was normalized to the average raw integrated density of control wild-type (WT) strain wells for each experiment. Biofilm formation ability was expressed as an average ratio of each mutant to the wild type for three independent experiments.

RESULTS

Transcriptome analysis of a Zur-deficient variant of *Anabaena* sp. PCC7120

RNA extracted from *Anabaena* sp. PCC7120 and Δ*zur* strains cultured until the mid-exponential growth phase was obtained and analysed by RNA-seq. A total of 405 genes, 6.6% of genes from the genome of *Anabaena* sp. PCC7120 were differentially expressed (fold change ≤ −2 or ≥2, FDR corrected *p*-value ≤0.05) between both strains. The overall distribution of DEGs against their statistical significance is shown in Figure S2. The volcano plot shows that the number of genes that displayed increased mRNA levels in the Δ*zur* strain (likely repressed by Zur, either directly or indirectly) compared to the WT *Anabaena* was much larger than those with diminished transcription (262 vs. 143, respectively). Although the data suggest that Zur preferentially works as a repressor in the cyanobacteria, it should be taken into account that many of these transcriptional changes may occur as a consequence of an indirect effect due to the lack of Zur, rather than being directly controlled by this regulatory protein. From these 405 genes, 218 were annotated and classified into different functional categories (Table 1), including metal transport and homeostasis, oxidative and general stress response, photosynthesis and respiration, carbohydrate metabolism, nitrogen metabolism, and heterocyst differentiation, cell wall synthesis, transport and binding proteins, ion efflux pumps and ion transporters, hydrogenases, amino acid metabolism, regulatory activities, transposases, and miscellaneous genes with different activities. Genes coding for hypothetical or unknown proteins are given in Table S2. The distribution of annotated genes according to functional categories that were differentially expressed presented in Figure 1 shows that the percentage of upregulated and downregulated genes varied markedly for each group. Metal transport and homeostasis, oxidative and general stress responses and carbohydrate metabolism contain mostly upregulated genes, while differently expressed genes of hydrogenases are downregulated. Functional categories with a major number of DEGs are discussed below.

Metal transport and homeostasis

In addition to the set of expected DEGs previously reported as Zur/FurB-targets (Napolitano et al., 2012), a series of novel genes involved in the homeostasis and transport of metals exhibited altered transcription in the Δ*zur* strain. Among them, the *smtB*-like repressor *aztR* (*all7621*) and the divergently transcribed Zn/Pb exporting ATPase *aztA* (*alr7622*) putatively involved in zinc homeostasis (Divya & Acharya, 2021; Napolitano et al., 2012) were upregulated. Also, a set of transporters involved in the homeostasis of other metals displayed altered transcription levels in the Δ*zur* strain, including the downregulation of several TonB-dependent iron transporters. This set of genes comprised *iacT* (Nicolaisen et al., 2010), the *alr2118-20* operon coding for the ferrous iron transport system FeoAB, the TonB-dependent transporter *alr4028-29*, which is induced under iron deficiency (Mirus et al., 2009), and the putative ferredoxin gene *alr4030*, which are organized in an operon with *fecB3* (*alr4031*), the latter taking part of the Fec system involved in Fe(III) uptake (Stevanovic et al., 2012). Besides, several genes putatively involved in copper homeostasis were downregulated, such as the *cusA* (*all7618*) and *cusB* (*all7619*) homologues (Nicolaisen et al., 2010) and the predicted operon *all7597*-92 comprising the copper exporter CopM homologue (*all7594*), a hypothetical protein (*all7593*) and the putative PIB1-type copper exporter (*all7592*) (Argüello et al., 2007; Giner-Lamia et al., 2015). On the other hand, the predicted operon *alr3947-48* that encodes the cobalt/nickel transport permease system CbiMQ (Fresenborg et al., 2020; Huertas et al., 2014) was upregulated. Additionally, several genes coding for transporters and porins, including several Na^+/H^+ antiporters and ABC transporters displayed altered transcription.

Photosynthetic and respiratory electron transport

The expression of some genes involved in photosynthesis and respiration was deregulated in the *zur* defective strain, being the *hoxEF* (*alr0751* and *alr0752*) and *hoxUYH* (*alr0762*, *alr0764* and *alr0766*) operons, encoding the bidirectional hydrogenase the most affected (Tamagnini et al., 2002). In *Synechocystis* sp. PCC 6803, the Hox complex mediates redox reactions with soluble electron carriers (i.e., NAD(P)H,

TABLE 1 Genes with known function differentially expressed in Δ*zur* strain related to the wild-type strain *Anabaena* sp. PCC7120.

ORF[a]	Gene name/protein description[b]	Fold change	Predicted Zur box	EMSA[c]
Metal transport and homeostasis				
all0830	*znuC*; ABC-transporter permease protein	5.26	+	+
*all0832**	*znuB*; ABC-transporter ATP-binding	95.41		+ (*all0833*)
*all0833**	*znuA*; periplasm soluble binding protein	46.24	+	+
*alr1197**	Putative metallochaperone	13.65	+	
*alr1198**	Metallophosphoesterase	12.89		
*alr1199**	Metallophosphatase	8.16		
all1751	Putative metallochaperone	2.1	+	
*alr2118**	Putative FeoBs protein, iron(II) transporter	−4.34	+	
*alr2119**	Putative FeoBs protein, iron(II) transporter	−5.67		
*asr2120**	Putative FeoBs protein, iron(II) transporter	−3.7		
asl2417	*atx1* homologue, copper chaperone	6.7		
all3161	Zn/Cd/Pb-exporting subgroup P_{IB2}, P-type ATPases	2.2		
*alr3242**	*hutA2*; haemoglobin/transferrin/lactoferrin receptor protein	53.8	+	+
*alr3243**	*fecB2*; ferrichrome ABC transporter, ferrichrome-binding protein	33.14		+ (*alr3242*)
all3515	metal binding and PEP-CTERM domains containing protein	119.18	+	
*alr3947**	*cbiM*; cobalt transport protein	2.47		
*alr3948**	*cbiQ*; cobalt transport protein	2.95		
all4026	*iacT*	−5.15		
alr4028[d]	Similar to vitamin B12 transport protein; fec system	15.85	+	[+]
alr4029[d]	Similar to vitamin B12 transport protein; fec system	35.3		
all4113	*pic1* homologue	7.5		
*all7592**	P_{IB1}-type copper exporters	−14.69		
*all7594**	*copM* homologue, copper transporter	−17.7		
all7610	*czcD*; Zn/Cd/Co- exporting CDF protein	−8.65	+	+
all7618	*cusA* homologue, copper transporter	−5.43	+	
all7619	*cusB* homologue, copper transporter)	−7.14		
all7621[e]	*aztR*; SmtB-like repressor	3.46	+	+
alr7622[e]	*aztA*; Zn/Pb exporting ATPase	2.79	+	+
alr7635	putative P_{IB1}-type copper exporter	4.74		
Oxidative and general stress response				
alr0286	*hsp17.1*; small heat shock protein	−3.51		
all0457	*lti46.3*; low temperature-induced protein	25.81		
all0458	*lti46.2*; low temperature-induced Dps protein homologue	19.46		
all0459	*lti46.1*; low temperature-induced protein	8.74		
all0634	Universal stress protein	−18.63		
asl0873	CAB/ELIP/HLIP superfamily protein	7.44	+	
all1173	Dps protein homologue	2.93	+	
alr1174	*rbrA*; rubrerythrin	2.5	+	−
all1495	*vapC2*; Type II toxin-antitoxin system	2.57		
all2096	*ptox*; oxidase	−4.04		
alr2204	*ntr*; thioredoxin reductase	4.03		
all2963	Oxidoreductase	3.63	+	−
all3034	Universal stress protein	−8.48		
asr3042	CAB/ELIP/HLIP superfamily protein	3.25		
asr3043	CAB/ELIP/HLIP superfamily protein	4.74		
alr3090	*catB*; Mn-catalase	9.12	+	

TABLE 1 (Continued)

ORF[a]	Gene name/protein description[b]	Fold change	Predicted Zur box	EMSA[c]
alr3199	Hemerythrin Dnase	14.4		
all4050	PRC barrel-like protein, UV-B radiation stress responsive	18.15		
all4051	PRC-barrel domain-containing protein	9.25		- (*all4052*)
asl4557	Rubredoxin	3.72		
alr5182	Oxidoreductase	15.17		
alr7354	Glutathione S-transferase	2.67		
Photosynthesis and respiration				
all0258	*petE*; plastocyanin precursor	3.15		
alr0348	*ndhD*; NADH dehydrogenase subunit 4	2.7		
all0801	Photosystem II protein W	−2.6		
all1123	NTD-OCP paralog	3.32		
all1258	*psbZ*; photosystem II 11 kD protein	−2.29	+	+
alr1450	*cyp110A1*; cytochrome P450	−5443.99		
all3221	NTD-OCP paralog	3.4	+	
alr3356	Similar to phytochrome	−2.59		
all3572	*psbAIV*; photosystem II protein D1	−4.98	+	
all3744	Probable phytoene dehydrogenase	3.35		
alr4251	*cytA*; c-type cytochrome	−3.07		
all4647	OCP protein AstaP homologues	3.19		
alr4733	*bchH*; Mg quelatase subunit H	3.39	+	−
alr4783	NTD-OCP paralog	7.92		
all4940	Homologue of the C-terminal domain of the OCP	6.57		
all5264	OCP protein AstaP homologues	2.7		
alr5314	Photosystem I P700 chlorophyll *a* apoprotein A2	2.28		
Carbohydrate metabolism				
*all0166**	*treS*; alpha-trehalase	17.11		– (*all0168*)
*all0167**	*mts1*; maltooligosyltrehalose synthase	16.94		– (*all0168*)
*all0168**	*mts2*; alpha-amylase	19.9		–
all0635	*ppsA*; phosphoenolpyruvate synthase	−13.78	+	+
all0875	Probable alpha-glucanotransferase	9.91	+	−
all0879	Alcohol dehydrogenase	2.63		
alr0895	Alcohol dehydrogenase	36.23	+	
alr0897	Alcohol dehydrogenase	32.76		+
alr1000	Probable glycosyl transferase	3.55		−
*all1058**	Kojibiose phosphorylase	5.69	+	+
*all1059**	*susB*; sucrose synthase	5.24		+ (*alr1058*)
alr1112	Probable transglycosylase	2.32	+	−
alr1911	*nifJ2*; pyruvate flavodoxin dehydrogenase	−6.83		−
all2285	Sugar transferase	3.14		+ (*all2293*)
*alr3069**	Probable glycosyl transferase	4.34		−
*alr3070**	Probable glycosyl transferase	3.8		– (*alr3069*)
*alr3071**	Probable glycosyl transferase	4.11		– (*alr3069*)
asr3089	Transglycosylase-associated protein	11.52		
all3735	*fbaB*; fructose-bisphosphate aldolase class I	4.01	+	−
alr3768	*orrA*; two-component response regulator	3.12		
alr3771	Aldehyde dehydrogenase	2.05	+	
all4052	Transketolase	19.26		−
asl4654	Transglycosylase-associated protein	10.86		
all4719	Similar to glucosyltransferase	2.16		−

(Continues)

TABLE 1 (Continued)

ORF[a]	Gene name/protein description[b]	Fold change	Predicted Zur box	EMSA[c]
alr4773	Alpha-glucosidase	3.06		+ (*alr4772*)
all4894	Thermostable β-glucosidase containing Fas-1 domain	2.18		
all4985	*susA*; sucrose synthase	2.66		
alr5331	alpha-glucosidase	3.83	+	+
all7335	6-phosphofructokinase	−2.33		
Nitrogen metabolism and heterocyst differentiation				
all0521	*patA*	−3.21		−
all1440[f]	*nifK*	6.83		− (*nifB*)
all1454[f]	*nifD*	−5.12		− (*nifB*)
all3035	Nitrate ABC transporter, ATP-binding protein	−11.73		−
all3036	Nitrate ABC transporter, permease inner membrane protein	−5.08		
*alr3233**	*trpE*; anthranilate synthase	−2.98		−
*alr3234**	Similar to heterocyst formation protein HetP	−5.21		−
all0571	*cphB2*; cyanophycinase	8.05		+
alr0573	*cphA2*; cyanophycin synthetase	2.85		
Cell wall				
alr0169	Cyclomaltodextrin glucanotransferase	12.13		
alr0248	*sjdR*; septal junction disk regulator	12.56	+	+
alr0834	Porin major outer membrane protein	3.37	+	+
alr3072	Probable polysaccharide biosynthesis protein	3.02		
alr3393	Similar to serum-resistance protein BrkB	7.23	+	
all3585	*tonB2*; TonB-like protein	13.01	+	
alr3659	Similar to S-layer-RTX protein	−2.5		−
all3983	Similar to surface layer protein	2.1		
all4539	L-sorbosone dehydrogenase	2.53		
alr5324	*anaPbp*; penicillin-binding protein	4.01		+
all7614	Porin OprB-like	−2.05		
Transport and binding proteins				
all0802	Putative MTS transporter	6.74	+	
all1110	Chromate transport protein	4.11	+	
alr1554	ABC transporter ATP-binding protein	2.77		
all1948	ABC transporter, ATP-binding protein	−2.47		
all3041	Putative MTS transporter	5.81		
all3310	BtuB transporter (TBDT)	−3.11	+	
all7609	Similar to heme binding protein CemA	−25.47		
Ion efflux pumps and ion transporters				
asl1840	*mnhF*; Na^+/H^+ antiporter subunit F	3.78		
all2113	Na^+/H^+ antiporter	2.79		
all3033	Ion efflux pumps and ion transporter homologue.	−3.7		
all3567	Probable Na^+/H^+-exchanging protein	2.52		
all4832	Similar to Na^+/H^+ antiporter	3.14		
alr5318	Potassium channel protein	4.1		
all5322	Similar to Na^+/H^+-exchanging protein	2.59		+
all7617	Similar to cation efflux system protein	−4.33		
Hydrogenases				
*alr0751**	*hoxE*; bidirectional hydrogenase, diophorase subunit	−8.26		
*alr0752**	*hoxF*; hydrogenase subunit	−11.83		
alr0762	*hoxU*; hydrogenase chain U	−3.41		
alr0764	*hoxY*; hydrogenase small subunit	−13.12		

TABLE 1 (Continued)

ORF[a]	Gene name/protein description[b]	Fold change	Predicted Zur box	EMSA[c]
alr0766	*hoxH*; hydrogenase large subunit	−11.77		
Amino acid metabolism				
*all0409**	*trpD*; anthranilate phosphoribosyltransferase	3.53		
*all0410**	*trpB*; tryptophan synthase beta subunit	3.72		
alr1414	*ahcY*; adenosylhomocysteinase	2.56		
alr1519	Amino acid transporter	3.37	+	
all3263	Histidine biosynthesis bifunctional protein; phosphoribosyl-AMP cyclohydrolase/phosphoribosyl-ATP pyrophosphohydrolase	2.18	+	
alr4784	Adenylosuccinate synthetase	2.47	+	[+]
alr7586	Cysteine synthase	−4.77	+	
Regulatory functions				
alr0072	Two-component response regulator	4.49		
*alr0428**	Two-component sensor histidine kinase	4.44		
*alr0429**	Two-component response regulator	5.47		
alr0900	Serine/threonine kinase with two-component sensor domain	3.15		
all0926	Two-component hybrid sensor and regulator	4.78		
*alr3165**	*asr*; bacteriorhodopsin	5.78	+	−
*alr3166**	*asrt*; sensory rhodopsin transducer	10.8		
*all3764**	Two-component hybrid sensor and regulator	2.69		
*all3765**	Two-component hybrid sensor and regulator	5.62	+	
*all3766**	Two-component response regulator	4.13		
*all3767**	Two-component sensor histidine kinase	4.52		
alr4329	Anti-sigma factor antagonist	2.8		
all4986	*ndhR orthologue*; low CO_2 responsive transcriptional regulator.	−3.97		
all5210	Two-component hybrid sensor and regulator	2.7		
all7218	Histidine kinase-like ATPase	−2.67		
alr7219	Two-component response regulator	−2.06		
*all7583**	Two-component sensor histidine kinase	−5.3		
*all7584**	Two-component response regulator	−3.15		+
*all7605**	Two-component sensor histidine kinase	−6.95		
*all7606**	Two-component response regulator	−9.36		
all7608	*sigB3*; group 2 sigma 70-type sigma factor	−83.23		
all7615	*sigB*; transcription initiation factor sigma	−10.61		
alr8535	Two-component response regulator	4.79		
Transposases				
all0016	Transposase	−10.99	+	
alr0553	Transposase	−12.67		
alr1859	Transposase	−7.02		
alr2683	Transposase	1144.84		
alr3610	Transposase	−8.12		
alr5157	Transposase	21.8		
alr7003	Transposase	−2.17		
all7105	Transposase	−6.48		
all7112	Transposase	−9.15	+	
all7178	Transposase	−3.2	+	
alr7228	Transposase	37.48		
asl7246	Transposase	−2.78		

(Continues)

TABLE 1 (Continued)

ORF[a]	Gene name/protein description[b]	Fold change	Predicted Zur box	EMSA[c]
all7268	Transposase	−5.56	+	
all7302	Transposase	−4.45		
alr7386	Transposase	−2.56		
Other				
ffs	7SL ncRNA	5.26		
alr0430	Probable short-chain dehydrogenase	2.72		
alr0731	Anaerobic ribonucleoside-triphosphate reductase activating protein	−6.32		
alr0765	CBS-CP12 domain protein	−16.61		
asr1131	*cse*; Ca^{2+} Sensor EF-hand	6.3		
alr1362	Putative carboxymethylenebutenolidase	2.36		
all1750	Similar to WD-repeat containing protein	3.13		
alr1912	Dihydroorotate dehydrogenase, chl pyrimidine biosynthesis	−5.61		
all2097	Cell death suppressor protein	2.63		
alr2104	Probable methyltransferase	3.27		
all2347	Naphthoate synthase	2.14		
alr3246	Pyridoxamine 5′ phosphate oxidase Related protein	6.73	+	
*all3315**	Thylakoid-anchored contractile injection system protein	−2.2		
*all3316**	Thylakoid-anchored contractile injection system protein	−3.01		
all3318	Thylakoid-anchored contractile injection system protein	−2.5		
asl3322	Thylakoid-anchored contractile injection system protein	−4.46		
all3324	Thylakoid-anchored contractile injection system protein	−3.4		
all3325	Thylakoid-anchored contractile injection system protein	−2.28		
alr3790	Rhodanese-related sulfurtransferase	6.8		
alr3828	*rimP*; ribosome maturation factor	2.32		
alr4512	Sulfide-quinone reductase	2.16		
*alr4526**	Similar to flotillin	−2.71		
*alr4528**	Similar to flotillin	−3.09		
alr4685	*ns1*; germacrene A synthase	−2.56	+	
*all4721**	*folE2*; GTP cyclohydrolase I	54.36		[+]
*all4722**	Similar to GTP-binding protein	60.41		
*all4723**	*thrS_2*; threonyl-tRNA synthetase	68.65	+	[+]
*all4724**	Similar to FAD-dependent oxidoreductase	46.72		
*all4725**	Delta-aminolevulinic acid dehydratase	88.93	+	[+]
alr4909	Similar to DNA repair protein rad25	2.31		
alr5303	*rplL*	3.24		
alr7132	mrr restriction system protein	−2.06		
all7316	Plasma membrane anchored PpiD homologue	−2.31		
all7348	Lethal leaf-spot 1 homologue	−2.17		
all7590	Isoprenylcysteine carboxyl methyltrans/phospholipid methyltransferase	−17.07	+	
allrs03	ssaA ncRNA	4.69		

[a]Contiguous genes in the table predicted to form an operon based on data from MicrobesOnline are marked with an asterisk (*).
[b]Gene name and protein description were annotated according to the databases CyanoBase (http://genome.microbedb.jp/cyanobase) and KEGG (http://genome.jp/kegg).
[c]Genes whose promoter region was tested by EMSA with FurB showing the result as +/−. FurB direct targets identified in previous works are denoted as [+].
[d]Note that *alr4028* and *alr4029* constitute one single open reading frame incorrectly annotated as two different ones.
[e]Divergently transcribed genes *alr7622* and *all7621* share a short (40 pb) intergenic region containing the FurB box, EMSA results could be associated to either or both.
[f]Please, note that in our culture conditions (presence of combined nitrogen) the *nifD* gene is interrupted by the 11.28 kb genetic element (Golden et al., 1991) and, in turn, the *nifHDK* cluster is not working as an operon. The putative transcription start sites (TSSs) for the *Anabaena* sp. PCC7120 *nif* cluster are found upstream *nifB*, *nifH*, *hesA* and *fdxH*. In this work, EMSA assays were carried out for the promoter region of *nifB* on account of having the strong TSS considered to be the main drive for its transcription (Kumar et al., 2019).

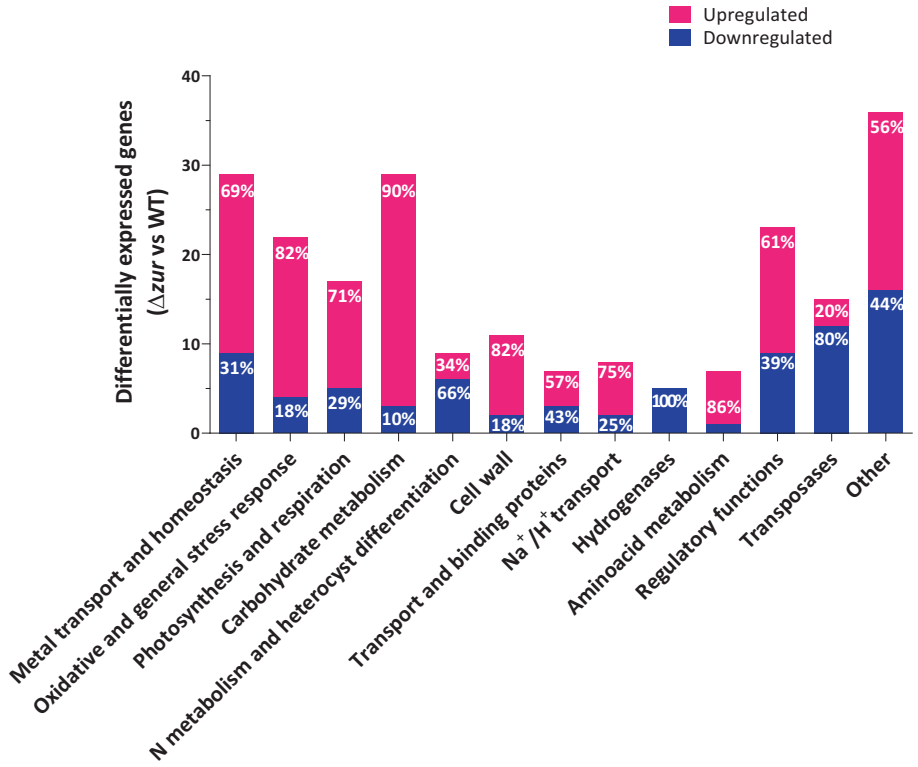

FIGURE 1 Functional annotation of the upregulated (pink) and downregulated (blue) genes in the Δ*zur* strain relative to *Anabaena* sp. PCC7120. Functional categories were described according to the databases CyanoBase (Fujisawa et al., 2017) and KEGG (Kanehisa et al., 2022).

ferredoxin, and flavodoxin), likely distributing peripheral electron flow from photosynthetic electron transfer to energy-transforming catalytic reactions not yet identified (Artz et al., 2020). Both *hox* operons are regulated by LexA (Sjoholm et al., 2007).

Nitrogen metabolism and heterocyst differentiation

Changes in the transcription of relevant genes involved in nitrogen metabolism and heterocyst differentiation were also observed. While transcript levels of *nifK* were enhanced, all other genes included in this set were downregulated in the *zur* deletion mutant. These genes included *all3035*, the ATP-binding protein of nitrate ABC transporter and the operon *alr3233-alr3234*, which is involved in the regulation of heterocyst differentiation and encodes the anthranilate synthase *trpE* and an *hetP* homologue (Videau et al., 2015; Videau et al., 2016). In addition, the transcript levels of the *patA* gene that is required for a correct heterocyst pattern formation (Liang et al., 1992) and the nitrogenase molybdenum-iron protein alpha chain *nifD* (Table S3) diminished in the *zur* deletion mutant. Conversely, the expression of the cyanophycinase and cyanophycin synthetase gene cluster encoding CphB2 and CphA2 was markedly increased (Picossi et al., 2004).

Amino acid metabolism

Transcription of most DEGs belonging to this functional category was slightly enhanced in the absence of Zur. In contrast, the cysteine synthase *alr7586* displayed a strong decrease in the *zur* defective strain.

Regulatory functions

Changes in the transcription of 23 genes involved in regulatory functions were detected, most of them encoding two-component systems, whose knowledge of cyanobacteria is rather poor. Most genes encoding two-component systems were organized in operons (10 genes out of 15) and 6 of them are located in plasmids. Well-characterized regulatory genes whose transcription diminished in Δ*zur* cells included the *ndhR* orthologue in *Anabaena* (*all4986*), which is involved in the control of CO_2 and HCO_3^- acquisition (Gollan et al., 2020; Wang et al., 2004), as well as the group 2 σ-factors *sigB* (*all7615*) and *sigB3* (*all7608*) which are also contained in plasmids (Ehira & Miyazaki, 2015).

Conversely, the transcription of the bacteriorhodopsin *asr* (*alr3165*) gene increased in the absence of Zur.

Oxidative and general stress response and detoxification

A set of genes involved in the oxidative stress response and detoxification exhibited increased transcription in the *zur* deletion mutant. Among the most affected were the *lti46* (low temperature-induced) and the *all4050-4051* (PRC-barrel-like proteins) operons, the oxidoreductase *alr5182*, the Mn-catalase *catB* (*alr3090*) as well as *all3034* and *all0634*, both encoding universal stress proteins. Genes induced by desiccation stress, such as those involved in trehalose biosynthesis, were not included in this functional category, since most of them are known to be involved in several, different metabolic pathways.

Carbohydrate metabolism

Interestingly, a high number of genes ($n = 29$) related to the carbohydrate metabolism category exhibited transcriptional changes in the absence of Zur, some of them arranged in clusters and operons (Figure S3). We observed a strong upregulation of the operon *all0168-66*. These genes are involved in trehalose metabolism and, as mentioned previously, they are markedly up-regulated upon dehydration and saline stress (Higo et al., 2006; Katoh et al., 2004). Tables 1 and S2 show that a large number (around 26%) of DEGs are related to desiccation tolerance or induced by desiccation stress. A comparison of our data with those reported by Higo et al. and Katoh et al. (Higo et al., 2006; Katoh et al., 2004) unveiled that around 50% of the genes that are up-regulated by dehydration (107 out of 209 genes) also displayed changes in the transcriptome of Δ*zur* cells, with 101 out these 107 genes being upregulated in the absence of Zur (Figure S4 and Table S4).

Upregulation of the sucrose synthase genes and fructose bisphosphate aldolase (*all3735*) was observed in the absence of Zur. In contrast, the transcription of the glycolytic enzyme phosphoenolpyruvate synthase (*all0635*) is strongly downregulated in the *zur* deletion mutant, as well as the pyruvate flavodoxin dehydrogenase gene *nifJ2* (*alr1911*). Considering the size of the potential Zur regulon, there is a remarkable number of genes involved in the transference of saccharide moieties (14 genes) whose transcription increases in the Δ*zur* strain. Most of them correspond to glycosyltransferases (8 genes) potentially involved in the synthesis of exopolysaccharides, the major component of bacterial biofilms (Rossi & De Philippis, 2015). Thus, transcription of the probable glycosyl transferases *alr3069, alr3070* and *alr3071* was enhanced in the Δ*zur* variant. These genes are part of a large cluster (Figure S3) that spans from *alr3057* to *alr3074* and encodes a set of proteins involved in polysaccharide biosynthesis and transport, including members of the Wzy-dependent pathway (Pereira et al., 2009). It is also noteworthy the strong increase in the transcription of the oxidoreductase *alr5182*, the putative alpha-glucanotransferase *all0875*, and the transketolase *all4052*. These genes have also been related to desiccation tolerance and, in turn, to changes in the synthesis of several glycosyl transferases (Katoh, 2012; Yoshimura et al., 2007; Yoshimura et al., 2012).

Transposases

Although differential transcriptomics unveiled 15 genes coding for transposases which showed altered gene expression, these data should be taken with caution. It should be taken into account that despite being annotated with different gene numbers, some of these transposases exhibited identical sequences. Therefore RNA-seq reads might not be associated with a single gene. Furthermore, 9 of these transposase genes are harboured in plasmids and it was recently reported that plasmid genes may suffer genome rearrangements in mutant strains of *Anabaena* sp. PCC7120 (Camargo et al., 2021).

Validation of RNA-Seq analysis

To validate the results obtained in RNA-seq, the expression level of 10 genes belonging to different functional categories was monitored by Real Time RT-PCR in strains Δ*zur* and *Anabaena* sp. PCC7120 (Figure 2). The selected genes were *ndhR*, *iacT*, *nifJ*, *hoxY*, *mts2*, *all4724*, *petE*, *rbrA, asr3089* and *all2285*. Two biological and three technical replicates were assayed for each gene. The transcriptional profile of these genes was in good agreement with the RNA-seq data (Table S3).

Deletion of zur affects transition metal transport

Since transcriptomic analysis unveiled strong changes in genes involved in the uptake and transport of other metals besides zinc, the determination of relevant transition metals in *Anabaena* sp. PCC 7120 and the Δ*zur* strains was carried out. Table 2 shows that, in good concordance with the transcriptomic data, the absence of Zur not only results in increased zinc content but also affects the transport of several major essential metals for the cyanobacteria (i.e., iron and manganese), as well as other heavy metals, such as copper and nickel. These data evidence that Zur not only controls zinc

homeostasis but also influences other transition metal trafficking in the cyanobacteria.

Questing functions of hypothetical proteins affected in the absence of Zur

Several genes whose transcription was largely affected in the Δ*zur* strain corresponded to unknown or hypothetical proteins for which there is no annotated function in GenBank. Thus, we investigated the hypothetical function using experimental evidence from the literature on cyanobacteria or other related microorganisms. When no reports about the function of these genes were found, we used the KEGG database (Kanehisa et al., 2022) to seek whether the orthologues of these hypothetical proteins from *Anabaena* sp. PCC7120 displayed identities ≥75% and presented assigned functions. Information about operon predictions and the presence of predicted Zur boxes were also investigated according to the operon information tool from MicrobesOnline (Alm et al., 2005) and as described in the materials and methods section respectively. These analyses allowed us to identify relevant features of a number of proteins which are shown in Table S2. Remarkably, many of these genes encoded proteins with predictive functions in dehydration tolerance. Among them, the predicted operon *asl0163-alr0164*, coding for two putative-membrane proteins, is induced under desiccation (Higo et al., 2006). According to Pfam (Mistry et al., 2021), the predicted protein coded by *asl0163* contains a conserved proteolipid Pmp3 domain, while All0164 is a transmembrane protein exhibiting a phage holin domain. The primary function of holins is the transport of murein hydrolases across the cytoplasmic membrane to the cell wall, to facilitate the incorporation of a new cell wall precursor during cell wall synthesis. Deregulation of cell wall hydrolysis and transference of new precursor induces cell lysis (Catalão et al., 2013). A cluster of genes with outstanding changes in the Δ*zur* variant has been related to desiccation tolerance (Higo et al., 2006; Katoh et al., 2004) and spans from genes *all0891* to *alr0898* (Figure S3). There are two operons predicted in this cluster. In the first one (*alr0892* to *alr0895*) it has been identified that *alr0893* codes for a putative protease induced by dehydration and, according to Pfam, *alr0894* codes for a predicted protein that contains a polyketide cyclase/dehydrase and lipid transport domain. This is flanked at the 3′ site by the *alr0895* gene that encodes a zinc-binding alcohol dehydrogenase. The second operon harbours the *alr0897* gene coding for a second alcohol dehydrogenase flanked by two genes coding for unknown proteins which are also induced by desiccation.

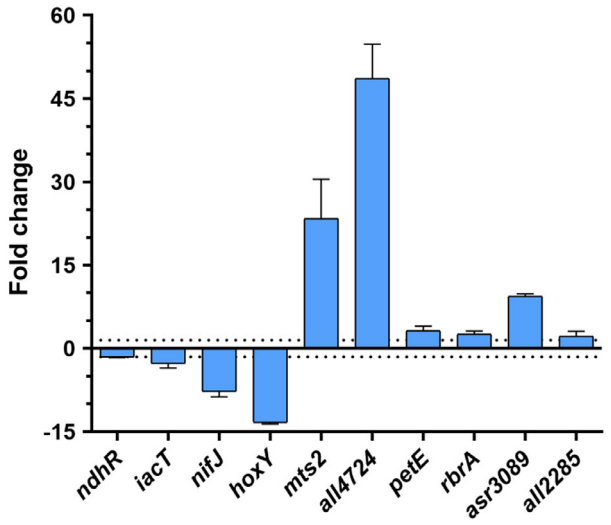

FIGURE 2 Validation of RNA-seq results of the Δ*zur* strain relative to *Anabaena* sp. PCC7120. Relative transcription of selected genes was determined by Real-Time RT-PCR. Values are expressed as fold change and correspond to the average of two biological and three technical replicates. The standard deviation is indicated.

Identification of regulatory motifs in potential Zur targets

To discriminate between direct Zur-targets and genes whose transcription was indirectly affected by the lack of Zur, the promoter regions of genes showing significative transcriptional changes were scanned for putative

TABLE 2 Inductively coupled plasma-mass spectrometric analysis for intracellular quantities of selected metals in the *Anabaena* sp. PCC7120 and Δ*zur* strains.

	Elements (metal quantity, mg/kg of cells)						
Strains	**Zn**	**Co**	**Cu**	**Fe**	**Mg**	**Mn**	**Ni**
WT	92.76 ± 30.83	7.10 ± 1.21	27.14 ± 6.8	1478.00 ± 454.68	246.00 ± 8.49	726.30 ± 173.64	0.72 ± 0.01
Δ*zur*	222.9 ± 10.92	10.52 ± 1.35	63.88 ± 5.9	3794.00 ± 339.79	295.50 ± 13.44	1327.00 ± 34.39	1.58 ± 0.23
Δ*zur*/WT means ratio	2.40	1.48	2.35	2.57	1.20	1.83	2.21
P-value	0.0302	0.0308	0.0287	0.0287	0.0479	0.0408	0.0326

Note: Results represent mean value and standard deviation for three independent biological replicates. Statistical significance was determined using the Holm-Sidak method, with a *p*-value cut-off of 0.05.

Zur-DNA binding motifs by FIMO analysis using a cut-off of a *p*-value $<1 \times 10^{-4}$. The position-weight-matrix generated by MEME with the Zur-DNA binding motifs reported previously (Napolitano et al., 2012) was used as input (Figure S1). The presence of Zur boxes in the tested promoters is indicated in Tables 1 and S2. To verify these predictions, EMSA was conducted with a selected set of DNA fragments amplified immediately upstream of differently expressed genes and that contained the promoter regions with potential Zur boxes. Around 72% of these fragments showed altered mobility in EMSA (Table 1 and representative results in Figure 3). Additionally, a potential direct regulation by Zur of a set of genes that showed outstanding changes in their transcription levels, or that could be related to zinc transport or desiccation processes, such as the *mts* operon, *nifJ2*, *all7609* and *alr5182* that encodes an oxidoreductase, among others, were also explored by EMSA, resulting negative (Table 1). However, despite the lack of predicted Zur boxes in the promoter of *alr0897* coding for alcohol dehydrogenase, an efficient interaction with Zur was observed via EMSA, while a weaker interaction of Zur with the promoters of the cyanophycinase *all0571* and the phosphoenolpyruvate synthase *all0635* was observed (Table 1 and Figure 3). Both promoter regions exhibited Zur potential binding motifs with a p-value near the $<1 \times 10^{-4}$ cutoff. It is noticeable that several genes involved in carbohydrate metabolism are direct targets of Zur, including *ppsA*, the operon containing *susB*, and the *all1058* phosphorylase genes, as well as the alpha-glucosidase genes *alr5331* and *alr4773*, the latter being placed in the same operon than the hypothetical protein Alr4772.

Deregulation of Zur strongly influences cell-to-cell aggregation and the formation of biofilms

In addition to the genes involved in zinc and metal transport, most chromosomal genes showing stronger transcriptional increases in the Δ*zur* strain were related to drought stress tolerance and carbohydrate metabolism. Most of these genes are involved in the biosynthesis of compatible solutes and polysaccharides, for example, several glycosyl transferases, transglycosylases and some other genes related to desiccation processes (Table 1). Since extracellular polysaccharides are important components of the matrix of the biofilm, we sought to investigate the effects of Zur de-regulation (lack or overexpression of this regulator) in the formation of *Anabaena* biofilms. After growing the cyanobacteria in static cultures on abiotic substrates, the planktonic cells were removed and adhered biofilms were visualized by crystal violet staining (Figure 4). Quantification of biofilms formed by the different *Anabaena* variants is given in Table 3. Interestingly, the adhered cells of the WT *Anabaena* were constituted by large cell aggregates dispersed between aggregates of medium a low size and single cells (Figure 4A). In contrast, the Δ*zur* mutant formed smaller aggregates than the parent strain while the biofilm biomass was drastically reduced (Figure 4B). Conversely, overexpression of Zur enhanced the size of the aggregates and the biofilm biomass (Figure 4C). Thus, our data point out that Zur production enhances biofilm formation.

Loss of Zur control affects heterocyst differentiation

Because carbon and nitrogen metabolic pathways are tightly coupled in *Anabaena* and a large number of genes involved in carbon metabolism are affected in the Δ*zur* strain, we decided to investigate whether the level of Zur in the cell could affect heterocyst development. In addition, despite not being direct Zur targets, our transcriptomic analysis unveiled a set of DEGs related to heterocyst differentiation and patterning, suggesting a potential alteration in the development of these specialized cells in the Δ*zur* and VCS2770 (Zur-overexpressing) *Anabaena* strains. Figure 5 and Table 4 show differences in heterocyst frequency among the three strains. Compared to the WT and VCS2770 strains, filaments of Δ*zur* cells contained the lowest percentage of heterocyst-like cells at semi-regular intervals which lacked red fluorescence. Interestingly, these potential heterocysts of Δ*zur* cells were not consistently stained by alcian blue, even after 72 h of nitrogen step-down (indicated with arrows in Figure 6). Alcian blue specifically reacts with the polysaccharide layer of pro-heterocysts and mature heterocysts. Therefore, in the absence of Zur, the differentiation of heterocysts appears incomplete. Conversely, the Zur overexpressing strain showed a modest increase in heterocyst frequency compared to the parent *Anabaena* sp. PCC7120 and could be easily stained with alcian blue.

DISCUSSION

As in most prokaryotes, Zur is the major regulator involved in the adaptation to zinc deficiency in cyanobacteria. However, because of the central role of zinc in the cell, it has been demonstrated that the deletion of *zur* not only affects the transcription of specific genes related to zinc uptake and transport but also a variety of genes coding for Zn-metalloproteins, metallochaperones, ABC transporters and outer membrane proteins (Napolitano et al., 2012). Our transcriptomic assays unveil novel relationships between Zur-deregulation and cyanobacterial metabolism. Our results evidence an interplay between zinc, iron and copper transport.

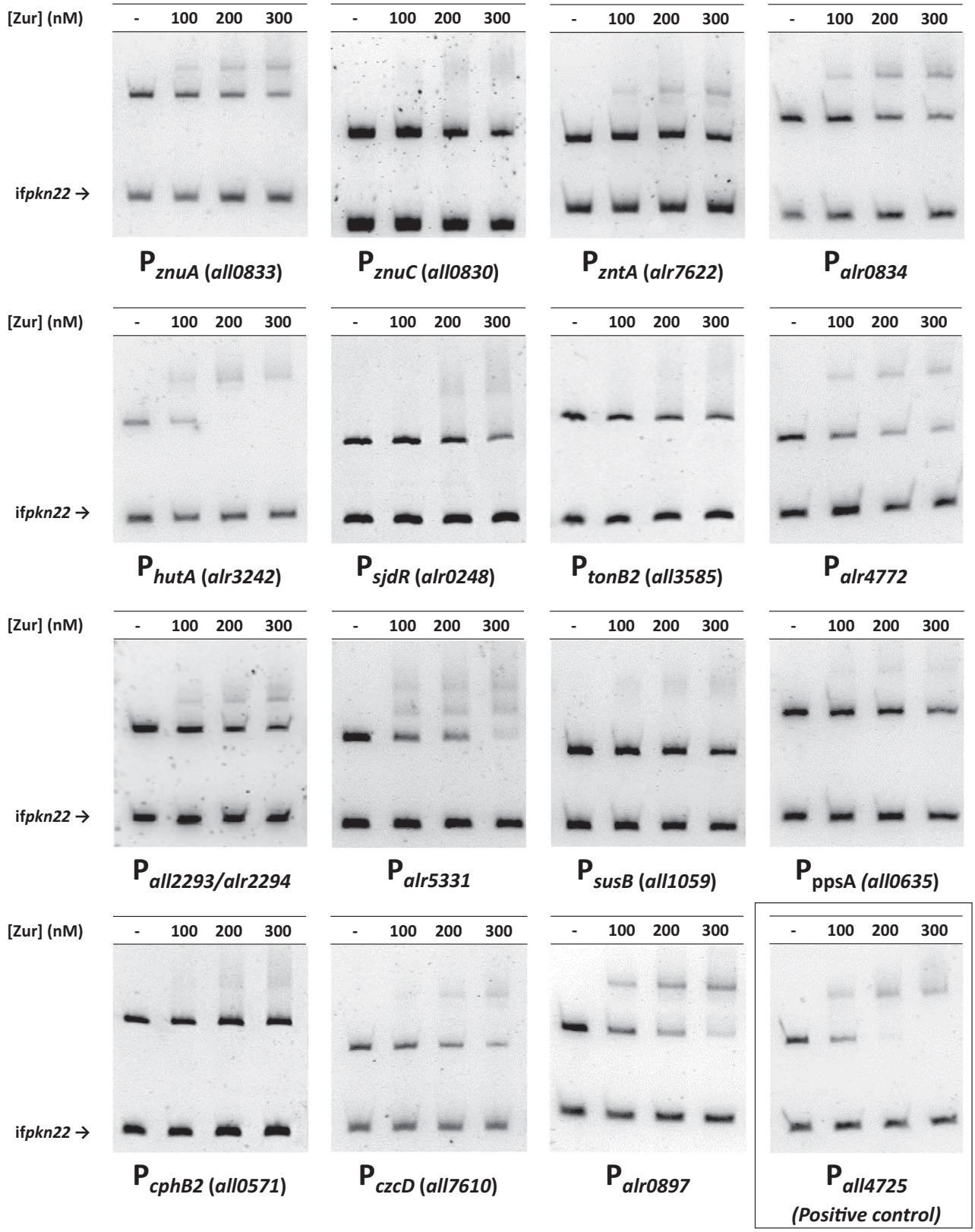

FIGURE 3 Electrophoretic mobility shift assays performed to test the in vitro interaction between Zur and the promoter regions of a selection of genes. All assays were performed with DNA fragments free or incubated along with the indicated increasing concentrations of Zur (nM), separated in 6% PAGE gels. The internal fragment of gene *pkn22* was used as non-specific competitor DNA. An electrophoretic mobility shift assay for the promoter region of gene *all4725* is included as a positive control.

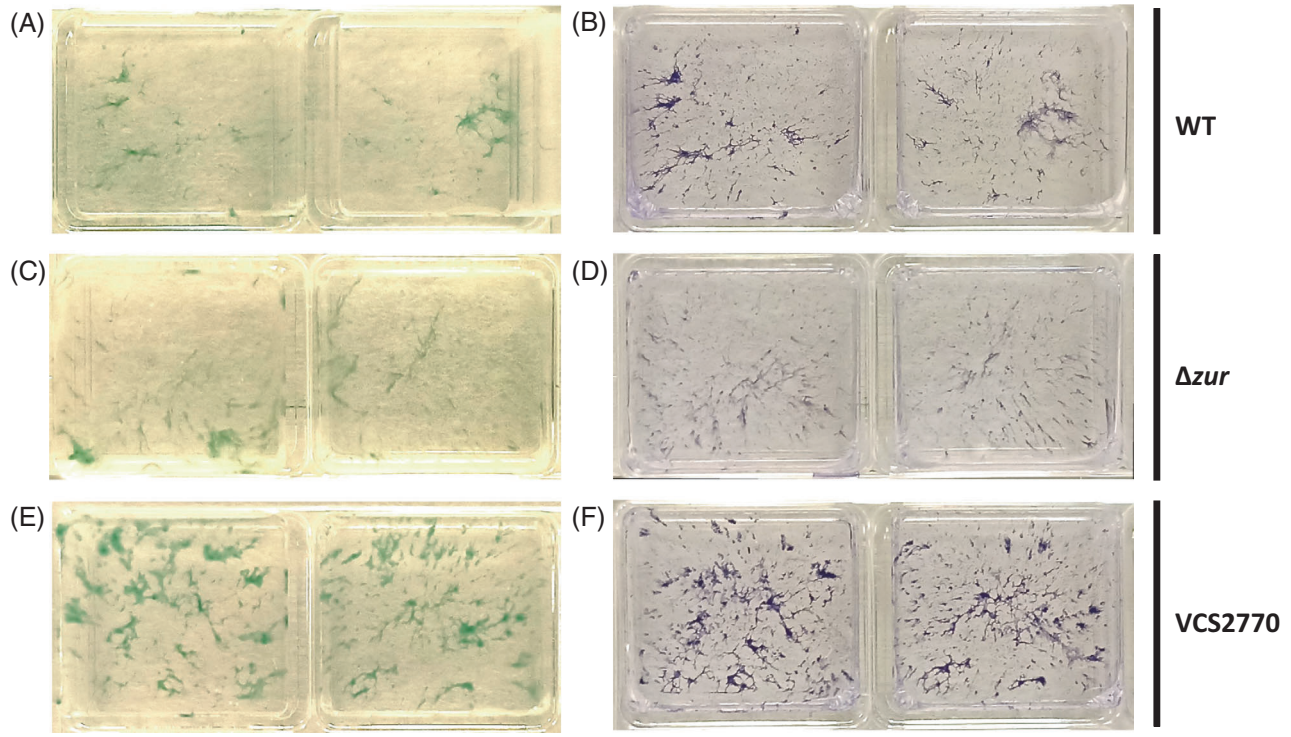

FIGURE 4 Biofilm formation by *Anabaena* sp. PCC7120 (A, B), Δ*zur* (C, D), and the VCS2770 Zur-overexpressing strain (E, F) after 10 days of culture as described in the Materials and Methods section. Panels A, C and E show biofilms before staining and B, D and F after staining with crystal violet.

TABLE 3 Biofilm formation by the Δ*zur* and Zur-overexpressing strains in relation to the wild-type strain after 10 days of static culture.

	Biofilm formation ratio (mutant/WT)			
Strain	**Experiment 1**	**Experiment 2**	**Experiment 3**	**Average ratio (*p*-value)**
VCS2770	1.35 ± 0.22	3.82 ± 1.34	1.26 ± 0.29	2.14 ± 1.44 (0.0466)
Δ*zur*	0.38 ± 0.06	0.31 ± 0.02	0.31 ± 0.09	0.35 ± 0.04 (2.2×10^{-5})

Note: Each individual experiment included two biological replicates. Statistical significance was determined using the Holm-Sidak method, with a *p*-value cut-off of 0.05.

Zur directly controls several components of the iron-transport machinery in *Anabaena*, as the transcription of the FeoB *alr2118-2120* operon whose transcription slightly diminishes in the Δ*zur* strain. Conversely, a strong increase in the transcription of the operon composed by the TonB-dependent receptor *hutA2* and the ferrichrome-binding protein *fecB2*, previously reported as Zur targets (Napolitano et al., 2012), has been observed (Table 1). Interestingly, several genes which encode hypothetical proteins (Table S2) are part of other operons involved in the siderophore cycling system and also present significantly increased transcription levels in the Δ*zur* strain. These genes include *all3586*, which lies upstream of *tonB2*; *alr4030* upstream of *fecB3* and *alr5330* which is in the 3′ side of *tonB4*. A complete map of these clusters can be found in (Stevanovic et al., 2012). This rise of transcription of the iron-uptake machinery in the absence of Zur is in good agreement with the higher content of iron detected by ICP in Δ*zur* cells. In addition, transcriptional changes of several porins and membrane proteins could somehow affect the permeability barrier for the uptake of metabolites, including other metals, such as nickel or copper. Several reports evidence the relationship between iron and copper transport in cyanobacteria (Nicolaisen et al., 2010; Zhen et al., 2021), as well as between zinc and copper (Badarau et al., 2013; Dainty et al., 2009). The higher intracellular content of copper in the Δ*zur* strain is in good concordance with the transcriptional decrease of several copper export systems, namely *czcD*, *cusAB*, and the operon containing *all7592* and the *copM* homologue *all7594*. In *Synechocystis* sp. PCC 6803 CopM is present in the periplasm and the extracellular space and its function remains controversial. It has been suggested that it could either prevent copper accumulation in the cell or assist in its transport outside the cell by a mechanism independent of the copper efflux system CopBAC

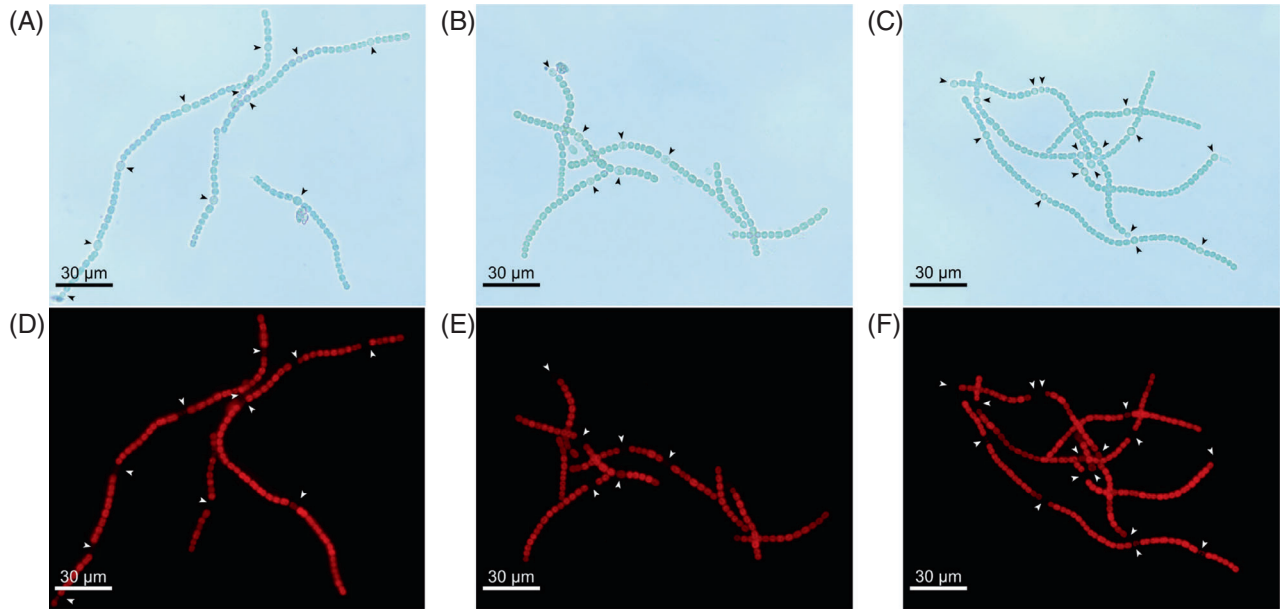

FIGURE 5 Presence of heterocysts in *Anabaena* sp. PCC7120 (A, D), Δ*zur* (B, E), and Zur overexpressing strains (C, F), as shown in representative micrographs taken after 72 h of combined nitrogen step-down. Corresponding fields shown under bright field (A, B, C) and fluorescence microscopy (D, E F) due to phycobiliprotein intrinsic fluorescence. Heterocysts are marked with arrowheads. Scale bars: 50 μm.

TABLE 4 Percentages of heterocysts present in cultures of *Anabaena* sp. PCC7120, Zur-overexpressing VCS2770 and Δ*zur* strains after 72 h of nitrogen step-down. Cells were counted in three biological replicates.

	% heterocysts			
Strain	**Experiment 1**	**Experiment 2**	**Experiment 3**	**Average % heterocysts (p-value)**
WT	8.2%	7.7%	8.4%	8.1 ± 0.4%
VCS2770	9.3%	8.1%	8.6%	8.7 ± 0.6% (0.2322)
Δ*zur*	5.3%	3.9%	4.3%	4.5 ± 0.7% ($2.2 \cdot 10^{-16}$)

Note: *P*-values represent the significance of the difference between the proportion of heterocysts developed by each of the mutant strains and the wild type, obtained through a 2-sample test for equality of proportions with continuity correction (R 4.2.2).

(Giner-Lamia et al., 2012). Interestingly, the transcription of *asl2417*, encoding the copper chaperone Atx1, increases in the absence of Zur. Atx1 can bind zinc in vivo with lower affinity than copper, linking copper and zinc homeostasis, though the function of the Atx1-Zn^{2+} interaction remains unclear (Dainty et al., 2009; Sazinsky et al., 2007). These results point to the occurrence of common players in a coordinated Fe-Cu-Zn transport, whose characterization would require further investigations. Similarly, the high content of nickel observed in the absence of Zur compared to the WT *Anabaena* could be due to a potential cross-talk between the cobalt and nickel uptake pathways to keep their homeostasis (Huertas et al., 2014) and is in good agreement with the transcriptomic data, which shows an increase in the transcription of the CbiMQ system (*alr3947-48*) in Δ*zur* cells. Additionally, the strong change in the expression of TonB2 and the porin coded by *alr0834* could also account for the higher content of Ni in the Δ*zur* strain. Nevertheless, though the mechanisms responsible for Ni and Co homeostasis have been widely investigated in the unicellular model *Synechocystis* sp. PCC 6803 (Huertas et al., 2014), the major players in *Anabaena* remain to be identified.

Among the transcriptional changes of genes involved in oxidative and general stress, the strong increase of the low-temperature induced Dps paralogs encoded by the lti46 operon (*all0457-all0459*) in the absence of Zur stands out. The Lti46.2/All0458 protein shows ferroxidase activity and is located in the cyanobacterial nucleoid, suggesting that it plays a DNA-protecting role (Sato et al., 2012). Interestingly, FurB/Zur has also been found to protect DNA by unspecific binding in vitro, and its overexpression in *E. coli* confers increased resistance to ROS (Lopez-Gomollon et al., 2009). The participation of Zur in the modulation of the oxidative stress response has also been reported (Sein-Echaluce et al., 2014). Our data shows a major number of genes involved in the stress response whose transcription is affected by the lack of Zur, including *catB* and several oxidoreductases. Other direct Zur targets, such as *sodA* and *gct3*

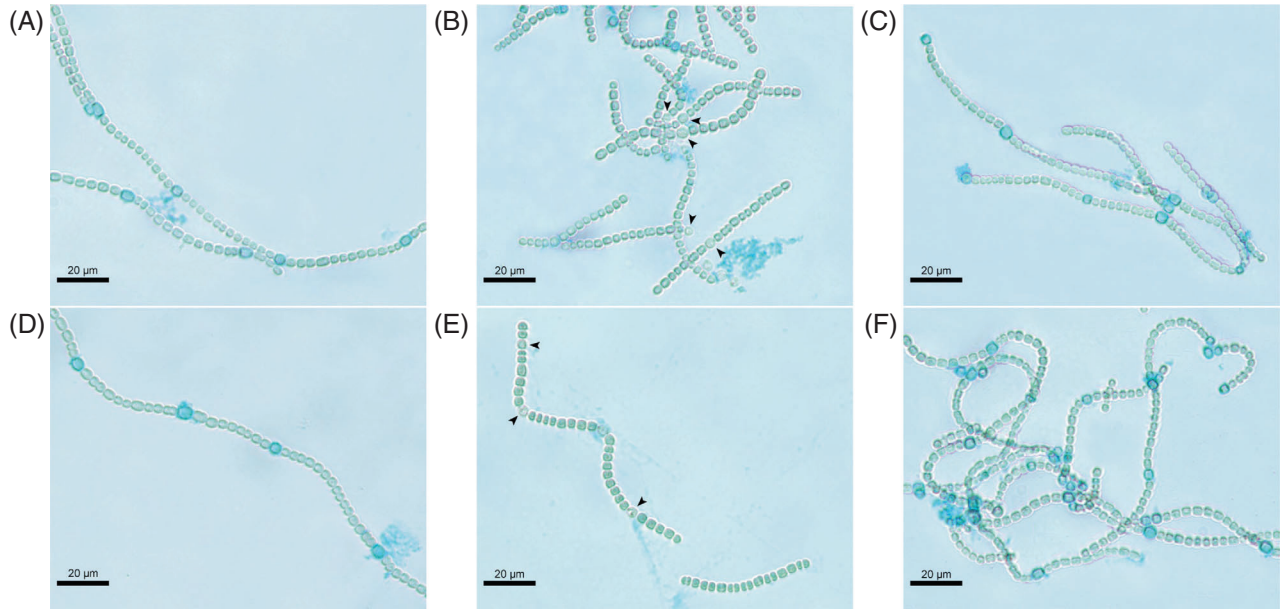

FIGURE 6 Representative bright field micrographs of *Anabaena* sp. PCC7120 (A, D), Δ*zur* (B, E), and Zur-overexpressing strains (C, F) grown 72 h under nitrogen deficiency and treated with alcian blue to stain the heterocyst polysaccharide layers. Black arrowheads indicate non-stained heterocysts.

(Sein-Echaluce et al., 2014) did not show significative differences in transcription when comparing Δ*zur* with the WT *Anabaena*, though Zur repression of these genes in the WT *Anabaena* may not take place under the standard culture conditions used in this work.

However, the most unexpected result of the transcriptomic data was the large number of genes involved in desiccation tolerance whose transcription increases and is severely affected in the Δ*zur* strain. Nevertheless, it should be noticed that most of those genes lack Zur-binding boxes (Table 1) and therefore are not likely to be direct Zur targets. Among them, the most affected genes are those involved in trehalose biosynthesis, which could help the cyanobacteria to withstand osmotic fluctuations (Asthana et al., 2005). Trehalose is synthesized by many organisms under different stress conditions, such as dehydration, saline environments, heat, oxidative stress and low temperatures (Asthana et al., 2008; Hayner et al., 2017). It is well known that mechanisms that protect cells from the effect of desiccation include those which circumvent oxidative damage (Shirkey et al., 2000). Therefore, it is likely to overlap among mechanisms of desiccation tolerance and response to oxidative stress imposed, for instance, by metal imbalance. Another strategy used by bacteria to survive desiccation and cope with different environmental stresses is the formation of biofilms (Bhattacharyya et al., 2021; Flemming et al., 2007). Bacterial cells in biofilms are also more resistant to adverse conditions, such as the presence of heavy metals and toxic chemicals (Parrilli et al., 2022). The higher sensitivity of the *zur* defective strain to oxidants (Sein-Echaluce et al., 2014) is in good concordance with its impaired ability to form biofilms. Conversely, biofilm formation by the Zur-overexpressing variant, which is more resistant to oxidative challenges, was more evident than in the wild-type *Anabaena*. Another reason which could account for the lower capability of Δ*zur* cells for developing biofilms is the decreased expression of the operon encoding the flotillin-like *alr4526* and *alr4528* genes. Flotillins are involved in the recruitment of proteins needed for functional lipid rafts, organizing signalling complexes and promoting the interactions of raft-associated proteins (Bramkamp & Lopez, 2015). Furthermore, many of those genes related to dehydration tolerance whose transcription is affected in the Δ*zur* strain encode cell-surface associated proteins and cell-wall proteins, as well as proteins involved in sugar metabolism which might be involved in biofilm formation (Table S4).

The strong transcriptional increase of the gene encoding the septal junction disk regulator SjdR, required for septal structure remodelling, is quite noticeable. An *Anabaena* mutant lacking SjdR showed impaired diazotrophic growth, with morphologically aberrant heterocysts which exhibited enhanced septal width and reduced cyanophycin plugs, among other atypical features (Schätzle et al., 2021). The increased transcription of *sjdR* in the Δ*zur* strain could be related to the narrower septa observed in Δ*zur* cells by scanning electron microscopy (Sein-Echaluce et al., 2014). Furthermore, the higher transcription of the cyanophycinase and cyanophycin synthetase gene cluster in Δ*zur* is also in good concordance with an increased

expression of *sjdR*. While *sjdR* lacks Zur boxes, we found that the *cphA2B2* cluster was directly modulated by Zur (Figure 3). Cyanophycin is a non-ribosomal polypeptide consisting of equimolar amounts of arginine and aspartate which works as a nitrogen/carbon reserve polymer. When grown in BG11 under different nitrogen regimes, cyanophycin accumulation mainly takes place through the activity of the NtcA-regulated CphA1-B1 cluster (Picossi et al., 2004), though the CphA2B2 proteins also play an important role in nitrogen metabolism under N_2-fixing conditions (Klemke et al., 2016). It could be speculated that the higher expression of *cphA2B2* in Δ*zur* cells could provide an additional synthesis of this dynamic nitrogen reservoir, which could alleviate the odd heterocyst differentiation.

It is worth noting that the transcriptomic profile of Δ*zur* shares some features with the transcriptional rearrangements observed in *Anabaena* after carbon stepdown (Gollan et al., 2020), namely the downregulation of the ferrous iron transporter subunits *alr2118-asr2120* and the *hox* clusters. The control of the carbon/nitrogen metabolic balance in cyanobacteria relies on signalling mechanisms triggered by 2-oxoglutarate and 2-phosp hoglycolate, which are sensed by CmpR and the repressor NdhR, whose transcription decreases dramatically in low CO_2 (Gollan et al., 2020; Zhang et al., 2018). A slight decrease in the transcription of the *ndhR* orthologue in *Anabaena* (*all4989*) has also been observed in Δ*zur* cells. Taking all those results together, it can be concluded that Zur deregulation not only affects metal homeostasis but also unbalances other metabolic pathways, influencing biofilm formation and leading to abnormal heterocyst development. Overall, our results unveil novel implications of the Zur regulon in the metabolism of *Anabaena* sp. PCC7120. Changes in the transcription of a plethora of genes involved in stress responses, including desiccation tolerance, appear to be the way the cyanobacteria copes with the additional stress imposed by the changes in metal content and the odd heterocyst envelope observed in the absence of Zur.

AUTHOR CONTRIBUTIONS

Irene Olivan-Muro: Investigation, experimental work and analysis of results; writing. **Cristina Sarasa Buisan:** Investigation, experimental work and analysis of results; writing. **Jorge Guio:** Methodology. **Jesús Arenas:** Methodology; editing the manuscript. **Emma Sevilla:** Conceptualization; methodology. **María F. Fillat:** Design of the work. Analysis of results, supervision; writing.

ACKNOWLEDGEMENTS

This work was funded by Ministerio de Ciencia, Innovación y Universidades (grant 438 PID2019-1048 89GB-I00) and from Gobierno de Aragón (grants E35_20R Biología Estructural).

CONFLICT OF INTEREST STATEMENT

The authors declare no conflicts of interest.

DATA AVAILABILITY STATEMENT

The RNA sequencing data are available in ArrayExpress with the accession number E-MTAB-12347. The authors confirm that the data supporting the findings of this study are available within the article [and/or] its supplementary materials.

ORCID

Cristina Sarasa-Buisan https://orcid.org/0000-0002-1960-2672
Emma Sevilla https://orcid.org/0000-0001-6435-3540
Maria F. Fillat https://orcid.org/0000-0001-8644-4574

REFERENCES

Alm, E.J., Huang, K.H., Price, M.N., Koche, R.P., Keller, K., Dubchak, I.L. et al. (2005) The MicrobesOnline web site for comparative genomics. *Genome Research*, 15(7), 1015–1022.

Argüello, J.M., Eren, E. & González-Guerrero, M. (2007) The structure and function of heavy metal transport P1B-ATPases. *Biometals*, 20(3), 233–248.

Artz, J.H., Tokmina-Lukaszewska, M., Mulder, D.W., Lubner, C.E., Gutekunst, K., Appel, J. et al. (2020) The structure and reactivity of the HoxEFU complex from the cyanobacterium Synechocystis sp. PCC 6803. *The Journal of Biological Chemistry*, 295(28), 9445–9454.

Asthana, R.K., Nigam, S., Maurya, A., Kayastha, A.M. & Singh, S.P. (2008) Trehalose-producing enzymes MTSase and MTHase in anabaena 7120 under NaCl stress. *Current Microbiology*, 56(5), 429–435.

Asthana, R.K., Srivastava, S., Singh, A.P., Kayastha, A.M. & Singh, S.P. (2005) Identification of maltooligosyltrehalose synthase and maltooligosyltrehalose trehalohydrolase enzymes catalysing trehalose biosynthesis in anabaena 7120 exposed to NaCl stress. *Journal of Plant Physiology*, 162(9), 1030–1037.

Badarau, A., Baslé, A., Firbank, S.J. & Dennison, C. (2013) Crosstalk between Cu(I) and Zn(II) homeostasis via Atx1 and cognate domains. *Chemical Communications*, 49(73), 8000–8002.

Bailey, T.L., Williams, N., Misleh, C. & Li, W.W. (2006) MEME: discovering and analyzing DNA and protein sequence motifs. *Nucleic Acids Research*, 34, W369–W373.

Barnett, J.P., Scanlan, D.J. & Blindauer, C.A. (2014) Identification of major zinc-binding proteins from a marine cyanobacterium: insight into metal uptake in oligotrophic environments. *Metallomics*, 6(7), 1254–1268.

Bhattacharyya, A., Pablo, C.H.D., Mavrodi, O.V., Weller, D.M., Thomashow, L.S. & Mavrodi, D.V. (2021) Rhizosphere plant-microbe interactions under water stress. *Advances in Applied Microbiology*, 115, 65–113.

Blindauer, C.A. (2008) Zinc-handling in cyanobacteria: an update. *Chemistry & Biodiversity*, 5(10), 1990–2013.

Bramkamp, M. & Lopez, D. (2015) Exploring the existence of lipid rafts in bacteria. *Microbiology and Molecular Biology Reviews*, 79(1), 81–100.

Camargo, S., Leshkowitz, D., Dassa, B., Mariscal, V., Flores, E., Stavans, J. et al. (2021) Impaired cell-cell communication in the multicellular cyanobacterium Anabaena affects carbon uptake, photosynthesis, and the cell wall. *iScience*, 24(1), 101977.

Catalão, M.J., Gil, F., Moniz-Pereira, J., São-José, C. & Pimentel, M. (2013) Diversity in bacterial lysis systems: bacteriophages show the way. *FEMS Microbiology Reviews*, 37(4), 554–571.

Chakraborty, S., Bhattacharjee, S., Tiwari, B., Jaishwal, T., Singh, S.S. & Mishra, A.K. (2022) Deciphering the mechanisms of zinc tolerance in the cyanobacterium *Anabaena sphaerica* and its zinc bioremediation potential. *Environmental Science and Pollution Research*, 30, 9591–9608.

CLC Genomics Workbench 12.0.3. (n.d.) Qiagen Bioinformatics. https://quiagenbioinformatics.com.

Cremers, C.M. & Jakob, U. (2013) Oxidant sensing by reversible disulfide bond formation. *Journal of Biological Chemistry*, 288(37), 26489–26496.

Dainty, S.J., Patterson, C.J., Waldron, K.J. & Robinson, N.J. (2009) Interaction between cyanobacterial copper chaperone Atx1 and zinc homeostasis. *JBIC Journal of Biological Inorganic Chemistry*, 15(1), 77–85.

De Magalhães, C.C.P., Cardoso, D., Dos Santos, C.P. & Chaloub, R.M. (2004) Physiological and photosynthetic responses of *Synechocystis aquatilis f. aquatilis* (cyanophyceae) to elevated levels of zinc. *Journal of Phycology*, 40(3), 496–504.

Decaria, L., Bertini, I. & Williams, R.J.P. (2010) Zinc proteomes, phylogenetics and evolution. *Metallomics*, 2(10), 706–709.

Divya, T.V. & Acharya, C. (2021) AzuR from the SmtB/ArsR family of transcriptional repressors regulates metallothionein in Anabaena sp. strain PCC 7120. *Frontiers in Microbiology*, 12, 782363.

Ehira, S. & Miyazaki, S. (2015) Regulation of genes involved in heterocyst differentiation in the cyanobacterium Anabaena sp. strain PCC 7120 by a group 2 sigma factor SigC. *Life (Basel)*, 5(1), 587–603.

Flemming, H.C., Neu, T.R. & Wozniak, D.J. (2007) The EPS matrix: the "house of biofilm cells". *Journal of Bacteriology*, 189(22), 7945–7947.

Fresenborg, L.S., Graf, J., Schätzle, H. & Schleiff, E. (2020) Iron homeostasis of cyanobacteria: advancements in siderophores and metal transporters. In: *Advances in cyanobacterial biology*. Cambridge, MA: Academic Press.

Fujisawa, T., Narikawa, R., Maeda, S.I., Watanabe, S., Kanesaki, Y., Kobayashi, K. et al. (2017) CyanoBase: a large-scale update on its 20th anniversary. *Nucleic Acids Research*, 45(D1), D551–D554.

Giner-Lamia, J., López-Maury, L. & Florencio, F.J. (2015) CopM is a novel copper-binding protein involved in copper resistance in Synechocystis sp. PCC 6803. *Microbiology*, 4(1), 167–185.

Giner-Lamia, J., López-Maury, L., Reyes, J.C. & Florencio, F.J. (2012) The CopRS two-component system is responsible for resistance to copper in the cyanobacterium Synechocystis sp. PCC 6803. *Plant Physiology*, 159(4), 1806–1818.

Golden, J.W., Whorff, L.L. & Wiest, D.R. (1991) Independent regulation of nifHDK operon transcription and DNA rearrangement during heterocyst differentiation in the cyanobacterium Anabaena sp. strain PCC 7120. *Journal of Bacteriology*, 173(22), 7098–7105.

Gollan, P., Muth-Pawlak, D. & Aro, E.-M. (2020) Rapid transcriptional reprogramming triggered by alteration of the carbon/nitrogen balance has an impact on energy metabolism in Nostoc sp. PCC 7120. *Life*, 10, 297.

Gonzalez, A., Bes, M.T., Barja, F., Peleato, M.L. & Fillat, M.F. (2010) Overexpression of FurA in anabaena sp. PCC 7120 reveals new targets for this regulator involved in photosynthesis, iron uptake and cellular morphology. *Plant & Cell Physiology*, 51(11), 1900–1914.

Grant, C.E., Bailey, T.L. & Noble, W.S. (2011) FIMO: scanning for occurrences of a given motif. *Bioinformatics*, 27(7), 1017–1018.

Hayner, G.A., Khetan, S. & Paulick, M.G. (2017) Quantification of the disaccharide Trehalose from biological samples: a comparison of analytical methods. *ACS Omega*, 2(9), 5813–5823.

Higo, A., Katoh, H., Ohmori, K., Ikeuchi, M. & Ohmori, M. (2006) The role of a gene cluster for trehalose metabolism in dehydration tolerance of the filamentous cyanobacterium Anabaena sp. PCC 7120. *Microbiology (Reading)*, 152(Pt 4), 979–987.

Huertas, M.J., Lopez-Maury, L., Giner-Lamia, J., Sanchez-Riego, A.M. & Florencio, F.J. (2014) Metals in cyanobacteria: analysis of the copper, nickel, cobalt and arsenic homeostasis mechanisms. *Life (Basel)*, 4(4), 865–886.

Kanehisa, M., Furumichi, M., Sato, Y., Kawashima, M. & Ishiguro-Watanabe, M. (2022) KEGG for taxonomy-based analysis of pathways and genomes. *Nucleic Acids Research*, 51, gkac963.

Katoh, H. (2012) Desiccation-inducible genes are related to N(2)-fixing system under desiccation in a terrestrial cyanobacterium. *Biochimica et Biophysica Acta*, 1817(8), 1263–1269.

Katoh, H., Asthana, R.K. & Ohmori, M. (2004) Gene expression in the cyanobacterium anabaena sp. PCC7120 under desiccation. *Microbial Ecology*, 47(2), 164–174.

Klemke, F., Nürnberg, D.J., Ziegler, K., Beyer, G., Kahmann, U., Lockau, W. et al. (2016) CphA2 is a novel type of cyanophycin synthetase in N2-fixing cyanobacteria. *Microbiology*, 162(3), 526–536.

Kumar, K., Ota, M., Taton, A. & Golden, J.W. (2019) Excision of the 59-kb fdxN DNA element is required for transcription of the nifD gene in Anabaena PCC 7120 Heterocysts. *New Zealand Journal of Botany*, 57(2), 76–92.

Liang, J., Scappino, L. & Haselkorn, R. (1992) The patA gene product, which contains a region similar to CheY of *Escherichia coli*, controls heterocyst pattern formation in the cyanobacterium Anabaena 7120. *Proceedings of the National Academy of Sciences of the United States of America*, 89(12), 5655–5659.

Livak, K.J. & Schmittgen, T.D. (2001) Analysis of relative gene expression data using real-time quantitative PCR and the 2 (-Delta Delta C(T)) method. *Methods*, 25(4), 402–408.

Lopez-Gomollon, S., Sevilla, E., Bes, M.T., Peleato, M.L. & Fillat, M.F. (2009) New insights into the role of fur proteins: FurB (All2473) from anabaena protects DNA and increases cell survival under oxidative stress. *The Biochemical Journal*, 418(1), 201–207.

Maret, W. (2006) Zinc coordination environments in proteins as redox sensors and signal transducers. *Antioxidants & Redox Signaling*, 8(9–10), 1419–1441.

Maret, W. (2019) The redox biology of redox-inert zinc ions. *Free Radical Biology and Medicine*, 134, 311–326.

McKinney, R. (1953) Staining bacterial polysaccharides. *Journal of Bacteriology*, 66(4), 453–454.

Mirus, O., Strauss, S. & Nicolaisen, K. (2009) TonB-dependent transporters and their occurrence in cyanobacteria. *BMC Biology*, 7, 68. https://doi.org/10.1186/1741-7007-7-68

Mistry, J., Chuguransky, S., Williams, L., Qureshi, M., Salazar Gustavo, A., Sonnhammer, E.L.L. et al. (2021) Pfam: the protein families database in 2021. *Nucleic Acids Research*, 49(D1), D412–D419.

Morel, F.M.M., Reinfelder, J.R., Roberts, S.B., Chamberlain, C.P., Lee, J.G. & Yee, D. (1994) Zinc and carbon co-limitation of marine phytoplankton. *Nature*, 369(6483), 740–742.

Napolitano, M., Rubio, M.A., Santamaria-Gomez, J., Olmedo-Verd, E., Robinson, N.J. & Luque, I. (2012) Characterization of the response to zinc deficiency in the cyanobacterium Anabaena sp. strain PCC 7120. *Journal of Bacteriology*, 194(10), 2426–2436.

Nicolaisen, K., Hahn, A. & Valdebenito, M. (2010) The interplay between siderophore secretion and coupled iron and copper transport in the heterocyst-forming cyanobacterium Anabaena sp. PCC 7120. *Biochimica et Biophysica Acta*, 1798, 1798–2140.

Outten, C.E. & O'Halloran, V.T. (2001) Femtomolar sensitivity of metalloregulatory proteins controlling zinc homeostasis. *Science*, 292(5526), 2488–2492.

Palenik, B., Brahamsha, B., Larimer, F.W., Land, M., Hauser, L., Chain, P. et al. (2003) The genome of a motile marine Synechococcus. *Nature*, 424(6952), 1037–1042.

Parrilli, E., Tutino, M.L. & Marino, G. (2022) Biofilm as an adaptation strategy to extreme conditions. *Rendiconti Lincei Scienze Fisiche e Naturali*, 33(3), 527–536.

Pereira, S., Zille, A., Micheletti, E., Moradas-Ferreira, P., De Philippis, R. & Tamagnini, P. (2009) Complexity of cyanobacterial exopolysaccharides: composition, structures, inducing factors and putative genes involved in their biosynthesis and assembly. *FEMS Microbiology Reviews*, 33(5), 917–941.

Perez, J.L. & Chu, T. (2020) Effect of zinc on *Microcystis aeruginosa* UTEX LB 2385 and its toxin production. *Toxins*, 12(2), 92.

Picossi, S., Valladares, A., Flores, E. & Herrero, A. (2004) Nitrogen-regulated genes for the metabolism of Cyanophycin, a bacterial nitrogen reserve polymer: expression and mutational analysis of two cyanophycin synthetase and cyanophycinase gene clusters in the heterocyst-forming cyanobacterium Anabaena sp. PCC 7120. *Journal of Biological Chemistry*, 279(12), 11582–11592.

Rossi, F. & De Philippis, R. (2015) Role of cyanobacterial exopolysaccharides in phototrophic biofilms and in complex microbial mats. *Life*, 5(2), 1218–1238.

Sánchez-Baracaldo, P., Bianchini, G., Wilson, J.D. & Knoll, A.H. (2022) Cyanobacteria and biogeochemical cycles through earth history. *Trends in Microbiology*, 30(2), 143–157.

Sarasa-Buisan, C., Guio, J., Broset, E., Peleato, M.L., Fillat, M.F. & Sevilla, E. (2022) FurC (PerR) from Anabaena sp. PCC7120: a versatile transcriptional regulator engaged in the regulatory network of heterocyst development and nitrogen fixation. *Environmental Microbiology*, 24(2), 566–582.

Sato, N., Moriyama, T., Toyoshima, M., Mizusawa, M. & Tajima, N. (2012) The all0458/lti46.2 gene encodes a low temperature-induced Dps protein homologue in the cyanobacteria anabaena sp. PCC 7120 and Anabaena variabilis M3. *Microbiology (Reading)*, 158(10), 2527–2536.

Sazinsky, M.H., LeMoine, B., Orofino, M., Davydov, R., Bencze, K.Z., Stemmler, T.L. et al. (2007) Characterization and structure of a Zn^{2+} and [2Fe-2S]-containing copper chaperone from *Archaeoglobus fulgidus*. *The Journal of Biological Chemistry*, 282(35), 25950–25959.

Schätzle, H., Arévalo, S., Flores, E. & Schleiff, E. (2021) A TonB-like protein, SjdR, is involved in the structural definition of the intercellular septa in the heterocyst-forming cyanobacterium anabaena. *MBio*, 12(3), e0048321.

Schneider, C.A., Rasband, W.S. & Eliceiri, K.W. (2012) NIH image to ImageJ: 25 years of image analysis. *Nature Methods*, 9(7), 671–675.

Sein-Echaluce, V.C., Gonzalez, A., Napolitano, M., Luque, I., Barja, F., Peleato, M.L. et al. (2014) Zur (FurB) is a key factor in the control of the oxidative stress response in Anabaena sp. PCC 7120. *Environmental Microbiology*, 17, 2006–2017.

Sein-Echaluce, V.C., Pallares, M.C., Lostao, A., Yruela, I., Velazquez-Campoy, A., Luisa Peleato, M. et al. (2018) Molecular basis for the integration of environmental signals by FurB from anabaena sp. PCC 7120. *The Biochemical Journal*, 475(1), 151–168.

Shirkey, B., Kovarcik, D.P., Wright, D.J., Wilmoth, G., Prickett, T.F., Helm, R.F. et al. (2000) Active Fe-containing superoxide dismutase and abundant sodF mRNA in Nostoc commune (cyanobacteria) after years of desiccation. *Journal of Bacteriology*, 182(1), 189–197.

Sjoholm, J., Oliveira, P. & Lindblad, P. (2007) Transcription and regulation of the bidirectional hydrogenase in the cyanobacterium Nostoc sp. strain PCC 7120. *Applied and Environmental Microbiology*, 73(17), 5435–5446.

Stevanovic, M., Hahn, A., Nicolaisen, K., Mirus, O. & Schleiff, E. (2012) The components of the putative iron transport system in the cyanobacterium Anabaena sp. PCC 7120. *Environmental Microbiology*, 14(7), 1655–1670.

Tamagnini, P., Axelsson, R., Lindberg, P., Oxelfelt, F., Wunschiers, R. & Lindblad, P. (2002) Hydrogenases and hydrogen metabolism of cyanobacteria. *Microbiology and Molecular Biology Reviews*, 66(1), 1–20.

Videau, P., Cozy, L.M., Young, J.E., Ushijima, B., Oshiro, R.T., Rivers, O.S. et al. (2015) The trpE gene negatively regulates differentiation of heterocysts at the level of induction in Anabaena sp. strain PCC 7120. *Journal of Bacteriology*, 197(2), 362–370.

Videau, P., Rivers, O.S., Hurd, K., Ushijima, B., Oshiro, R.T., Ende, R.J. et al. (2016) The heterocyst regulatory protein HetP and its homologs modulate heterocyst commitment in Anabaena sp. strain PCC 7120. *Proceedings of the National Academy of Sciences of the United States of America*, 113(45), E6984–E6992.

Vioque, A. (1992) Analysis of the gene encoding the RNA subunit of ribonuclease P from cyanobacteria. *Nucleic Acids Research*, 20(23), 6331–6337.

Wang, H.L., Postier, B.L. & Burnap, R.L. (2004) Alterations in global patterns of gene expression in Synechocystis sp. PCC 6803 in response to inorganic carbon limitation and the inactivation of ndhR, a LysR family regulator. *The Journal of Biological Chemistry*, 279(7), 5739–5751.

Yoshimura, H., Ikeuchi, M. & Ohomori, M. (2012) Cell surface-associated proteins in the filamentous cyanobacterium Anabaena sp. strain PCC 7120. *Microbes and Environments*, 27(4), 538–543.

Yoshimura, H., Okamoto, S., Tsumuraya, Y. & Ohmori, M. (2007) Group 3 sigma factor gene, sigJ, a key regulator of desiccation tolerance, regulates the synthesis of extracellular polysaccharide in cyanobacterium Anabaena sp. strain PCC 7120. *DNA Research*, 14(1), 13–24.

Zhang, C.C., Zhou, C.Z., Burnap, R.L. & Peng, L. (2018) Carbon/nitrogen metabolic balance: lessons from cyanobacteria. *Trends in Plant Science*, 23(12), 1116–1130.

Zhen, Z.H., Qin, S., Ren, Q.M., Wang, Y., Ma, Y.Y. & Wang, Y.C. (2021) Reciprocal effect of copper and iron regulation on the proteome of Synechocystis sp. PCC 6803. *Frontiers in Bioengineering and Biotechnology*, 9, 673402.

SUPPORTING INFORMATION

Additional supporting information can be found online in the Supporting Information section at the end of this article.

How to cite this article: Olivan-Muro, I., Sarasa-Buisan, C., Guio, J., Arenas, J., Sevilla, E. & Fillat, M.F. (2023) Unbalancing Zur (FurB)-mediated homeostasis in *Anabaena* sp. PCC7120: Consequences on metal trafficking, heterocyst development and biofilm formation. *Environmental Microbiology*, 1–21. Available from: https://doi.org/10.1111/1462-2920.16434